

# NAVIDA: Vision-Language Navigation with Inverse Dynamics Augmentation

Weiyi Zhu<sup>1\*</sup> Zekai Zhang<sup>1\*</sup> Xiangchen Wang<sup>1\*</sup> Hewei Pan<sup>1</sup>  
 Teng Wang<sup>1</sup> Tiantian Geng<sup>1</sup> Rongtao Xu<sup>2,3</sup> Feng Zheng<sup>1,3†</sup>  
<sup>1</sup> SUSTech <sup>2</sup> MBZUAI <sup>3</sup> SpatialTemporal AI

## Abstract

*Vision-and-Language Navigation (VLN) requires agents to interpret natural language instructions and act coherently in visually rich environments. However, most existing methods rely on reactive state-action mappings without explicitly modeling how actions causally transform subsequent visual observations. Lacking such vision-action causality, agents cannot anticipate the visual changes induced by its own actions, leading to unstable behaviors, weak generalization, and cumulative error along trajectory. To address these issues, we introduce NAVIDA (Navigation with Inverse Dynamics Augmentation), a unified VLN framework that couples policy learning with action-grounded visual dynamics and adaptive execution. NAVIDA augments training with chunk-based inverse-dynamics supervision to learn causal relationship between visual changes and corresponding actions. To structure this supervision and extend the effective planning range, NAVIDA employs hierarchical probabilistic action chunking (HPAC), which organizes trajectories into multi-step chunks and provides discriminative, longer-range visual-change cues. To further curb error accumulation and stabilize behavior at inference, an entropy-guided mechanism adaptively sets the execution horizon of action chunks. Extensive experiments show that NAVIDA achieves superior navigation performance compared to state-of-the-art methods with fewer parameters (3B vs. 8B). Real-world robot evaluations further validate the practical feasibility and effectiveness of our approach. Code and data will be available upon acceptance.*

## 1. Introduction

Vision-and-Language Navigation (VLN) [3, 18, 32] is a challenging multimodal sequential decision-making task, requiring an agent to navigate effectively through a 3D visual environment based solely on natural language instructions. Accordingly, effective VLN requires not only precise instruction comprehension but also long-horizon temporal

\*Equal contribution

†Corresponding Author

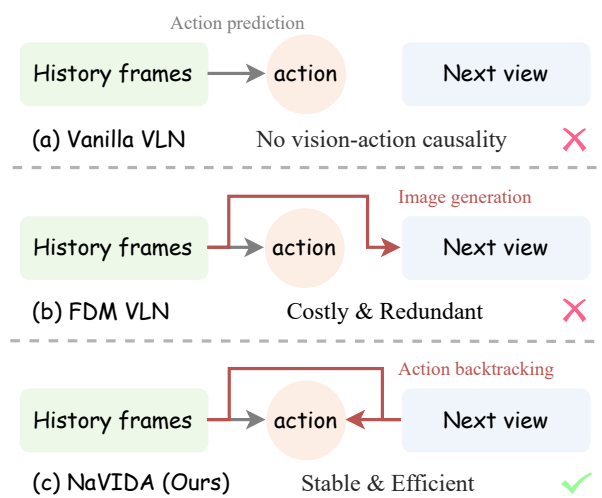


Figure 1. Comparison of three VLN paradigms. (a) Vanilla VLN relies on state-action mapping, lacking the causality between vision and actions; (b) Forward Dynamics Modeling (FDM) adds an additional image generation task which predicts future observations but is compute-heavy and distractible; (c) NAVIDA uses inverse dynamics supervision to learn the causality between vision and actions with the action prediction task only, making the learning process more efficient and stable.

modeling and robust generalization to visually diverse, unseen scenes. Motivated by advances in video-based Multimodal Large Language Models (MLLMs) [4, 23, 48], recent studies [8, 34, 39, 44, 46, 49] have integrated these models into VLN to exploit their superior visual perception, semantic understanding, and cross-scene generalization.

Many existing works [8, 44, 46] typically formulate VLN as a short-sighted state-to-action reactive strategy. As shown in Fig. 1(a), they map current language instruction and past visual observations to a few subsequent actions. This simplification ignores the potential causal relationships between visual information changes and corresponding actions in navigation tasks: *how current visual observations are transferred to the next visual observation through the influence of actions*. The model cannot predict the visual consequences of its actions, thus failing to correct small biases that gradually accumulate into serious nav-

igational instability, such as future viewpoint misalignment caused by slight premature turns. As shown in Fig. 1(b), recently some visual prediction-based works [16, 34, 47] combine forward dynamics modeling (FDM), attempting to use future observations as auxiliary signals for prediction, but such image generation tasks usually require additional prediction modules, such as diffusion-based world models [6, 9], which introduces additional computational burdens [31, 47] and causes the model to be confined to redundant details [37, 47].

To address these challenges, inspired by the inverse dynamic models (IDM), we propose NAVIDA, a VLN framework that integrates inverse-dynamics supervision (IDS) as an auxiliary signal to learn the causal relationship between visual changes and corresponding actions. This generates a language-independent visual motion concept, allowing the model to understand the physical consequences of its predicted actions without predicting dense image features, even if it cannot see the future frames. To provide IDS with richer and more discriminative learning signals, we introduce a hierarchical probabilistic action chunking (HPAC) mechanism that progressively merges low-level actions into multiple levels of action chunks. Specifically, we first group temporally adjacent atomic actions with consistent visual transition patterns into sub-chunks, and then further merge these sub-chunks into higher-level chunks, thus representing more complete and semantically coherent behavior. Such hierarchical mechanism allows the agent to predict over extended temporal horizons, leading to more stable navigation. Moreover, during inference, we propose an entropy-guided execution selection mechanism that adaptively adjusts the execution horizon of predicted action chunks according to their uncertainty, allowing for early re-planning and timely trajectory correction. Extensive experiments demonstrate that NAVIDA significantly enhances the causal understanding of visual actions, achieving state-of-the-art (SOTA) performance on the VLN-CE [18] benchmarks with fewer parameters, thus establishing a simple and lightweight paradigm for VLN research.

In summary, our contributions are threefold:

- We propose NAVIDA, a novel VLN framework that explicitly integrates inverse-dynamics supervision to learn causal relationship between visual changes and corresponding actions, enabling stable navigation behaviors.
- The NAVIDA adopts a HPAC mechanism to provide the inverse-dynamics supervision with richer and more discriminative learning signals, together with a dynamic entropy-guided execution horizon selection strategy to mitigate error accumulation during inference.
- Comprehensive experiments on VLN-CE benchmarks demonstrate that NAVIDA attains SOTA performance with fewer parameters, confirming the efficiency and effectiveness of our design and highlighting the value of

inverse dynamic modeling for VLN.

## 2. Related Work

**Vision-and-Language Navigation.** VLN tasks require an embodied agent to perceive, reason, and act in response to natural-language instructions. Early studies [7, 14, 22] focused on discrete navigation on connectivity graphs with panoramic RGB-D inputs, achieving strong in-domain results but relying on heavy sensors and pre-scanned viewpoints. Subsequent works [18, 40] have moved toward continuous control and low-level action prediction to better reflect real-world deployment, while several efforts [1, 11, 15, 25, 29, 30, 36] have investigated monocular RGB or RGB-D variants that relax reliance on panoramic sensing. Concurrently, the emergence of MLLMs has spurred monocular-only VLN systems that leverage vision-language backbones for stronger cross-scene transfer and lower hardware cost [8, 39, 44, 46]. Despite these advances, most VLN methods remain limited to reactive state-to-action mapping modeling, neglecting the potential causal relationship between changes in visual observation and corresponding actions. Lacking such causal grounding, agents struggle to anticipate visual consequences, which leads to unstable turning or stop behaviors and long-horizon error accumulation. In contrast, our NAVIDA explicitly encodes the action and induced visual change through inverse-dynamics supervision, enabling the policy to couple language grounding with short-horizon causal prediction and thereby stabilizing execution under monocular sensing.

**Dynamic Models in Navigation.** Reactive state-action modeling directly maps historical visual observations and natural language instructions to the action space, lacking causal modeling between changes in visual information and actions. To mitigate this, early works [12, 21, 41] explored using additional pre-training tasks such as path-mask prediction, image prediction, or image completion. However, these were mostly limited to discrete environmental settings and often relied on extended contextual cues or language instructions. More recent methods [16, 34, 47] attempted to combine forward dynamics modeling and decompose the decision task, predicting future images while simultaneously predicting actions. Although effective in some settings, forward models typically require additional modules for high-dimensional prediction, increase compute and memory, and can bias learning toward redundant appearance details that are weakly aligned with the decision space. NAVIDA instead adopts inverse dynamics in a continuous environment: from two adjacent images it directly infers the action that caused the transition, sharing the output space with the reactive policy and avoiding extra generators or decoders. This design reduces optimization difficulty in mapping from image space to action space, improves data efficiency, and injects a causal prior that strengthens instruc-

tion grounding, yielding stable long-horizon navigation.

### 3. NAVIDA Framework

#### 3.1. Preliminary

**Task Formulation.** The Vision-and-Language Navigation task in continuous environment is defined as follows. At the beginning of each navigation episode, the agent receives a natural language instruction  $\mathcal{I}$ . Then, at each time step  $t$ , the agent receives an egocentric RGB observation  $v_t$ ; we denote the observation history by  $\mathcal{V}_{0:t} = \{v_0, \dots, v_t\}$ . The discrete action space of the navigation agent is:

$$\mathcal{A} = \{\text{FORWARD}, \text{TURNLEFT}, \text{TURNRIGHT}, \text{STOP}\},$$

and selecting an action  $a_t \in \mathcal{A}$  triggers a transition to a new state and yields the next observation  $v_{t+1}$ . Episodes terminate when the agent issues `STOP` or reaches a maximum step budget  $T_{\max}$ . When the agent takes a stop action within 3 meters of the target position, the episode is considered successful.

**Framework Overview.** Motivated by the need to explicitly couple actions with the visual transitions they induce, we introduce NAVIDA on a standard VLM backbone consisting of a visual encoder, a vision–language projector, and an LLM head (Fig. 2). On this backbone, our NAVIDA is organized around three mutually consistent components: (i) a variable-length action representation via Hierarchical Probabilistic Action Chunking (HPAC), (ii) *inverse-dynamics supervision* (IDS) injected at the data level during training, and (iii) an *entropy-guided* rule at inference to adaptively choose the executed prefix. The chunk grammar aligns IDS and VLN in the same action space; IDS strengthens vision-action causality without adding modules; entropy-guided execution stabilizes decoding by aligning horizon with model confidence.

#### 3.2. Hierarchical Probabilistic Action Chunking

Instead of predicting a fixed small number of next actions, NAVIDA represents control as variable-length chunks to (a) amplify action-induced visual change for inverse-dynamic supervision and (b) allow farther-ahead decoding when confident, while keeping outputs consistent with the VLN action space. We use an HPAC mechanism to merge atomic actions in two stages. In the first probabilistic merging stage, up to 3 temporally adjacent and visually consistent repetitions of the same atomic action are merged into a sub-chunk with probability  $p$ , which compacts micro-motions and reduces label noise. In the second, deterministic merging stage, up to  $n$  consecutive sub-chunks are merged into a final chunk, yielding a sequence that covers between  $n$  and  $3n$  atomic actions. The resulting grammar preserves fine-grained short-range decisions while permitting farther-ahead decoding when confidence is high, and it amplifies

---

#### Algorithm 1 Hierarchical Probabilistic Action Chunking

**Require:** Atomic actions  $\mathcal{A} = [a_1, \dots, a_N]$ , merge prob.  $p$ , max level-2 chunk size  $n$   
**Ensure:** Hierarchically merged sequence  $\mathcal{A}^{(2)}$

**{Level-1: Probabilistic merging}**

- 1:  $\mathcal{A}^{(1)} \leftarrow [ ], c \leftarrow [a_1]$
- 2: **for**  $i = 2$  to  $N$  **do**
- 3:   **if**  $a_i = a_{i-1}$  and  $\text{len}(c) < 3$  and  $\mathcal{U}(0, 1) \leq p$  **then**
- 4:     Append  $a_i$  to  $c$
- 5:   **else**
- 6:     Append  $c$  to  $\mathcal{A}^{(1)}$ ;  $c \leftarrow [a_i]$
- 7:   **end if**
- 8: **end for**
- 9: Append  $c$  to  $\mathcal{A}^{(1)}$

**{Level-2: Deterministic merging}**

- 10:  $\mathcal{A}^{(2)} \leftarrow [ ], c' \leftarrow [\mathcal{A}_1^{(1)}]$
- 11: **for**  $i = 2$  to  $|\mathcal{A}^{(1)}|$  **do**
- 12:   **if**  $\text{len}(c') < n$  **then**
- 13:     Append  $\mathcal{A}_i^{(1)}$  to  $c'$
- 14:   **else**
- 15:     Append  $c'$  to  $\mathcal{A}^{(2)}$ ;  $c' \leftarrow [\mathcal{A}_i^{(1)}]$
- 16:   **end if**
- 17: **end for**
- 18: Append  $c'$  to  $\mathcal{A}^{(2)}$
- 19: **return**  $\mathcal{A}^{(2)}$

---

action-induced appearance and viewpoint changes, thereby producing more discriminative supervision signals. The complete procedure is summarized in Algorithm 1. This chunk representation is used as the training target, providing a unified label space for IDS and navigation action prediction, and supporting chunk-level uncertainty estimation used by the entropy-guided execution rule.

#### 3.3. Inverse-Dynamics Supervision

To reinforce the causal link between action and visual transition without modifying the architecture, we introduce inverse-dynamics supervision at the data level. Given an HPAC-induced pair of frames  $(v_t, v_{t+\ell})$ , the model is required to predict the token sequence of the intervening variable-length action chunk  $\mathbf{y}_t = (y_{t,1}, \dots, y_{t,n_t})$  using the same action grammar as VLN (i.e., action-type and numeric tokens). Supervision at the level of frame pairs and action chunks aggregates several micro-motions, leading to larger parallax and appearance changes and thus a more discriminative signal in settings with local aliasing (e.g., symmetry or transient occlusion). Following StreamVLN [39] and JanusVLN [43], we construct supervision data using Habitat [28] trajectories from R2R [3], RxR [20], ScaleVLN [35] and DAgger [27]. For each trajectory we use HPAC to define waypoints, and adjacent waypoints define non-overlapping subsequences, where the start frame is stored as the current view, the end frame as

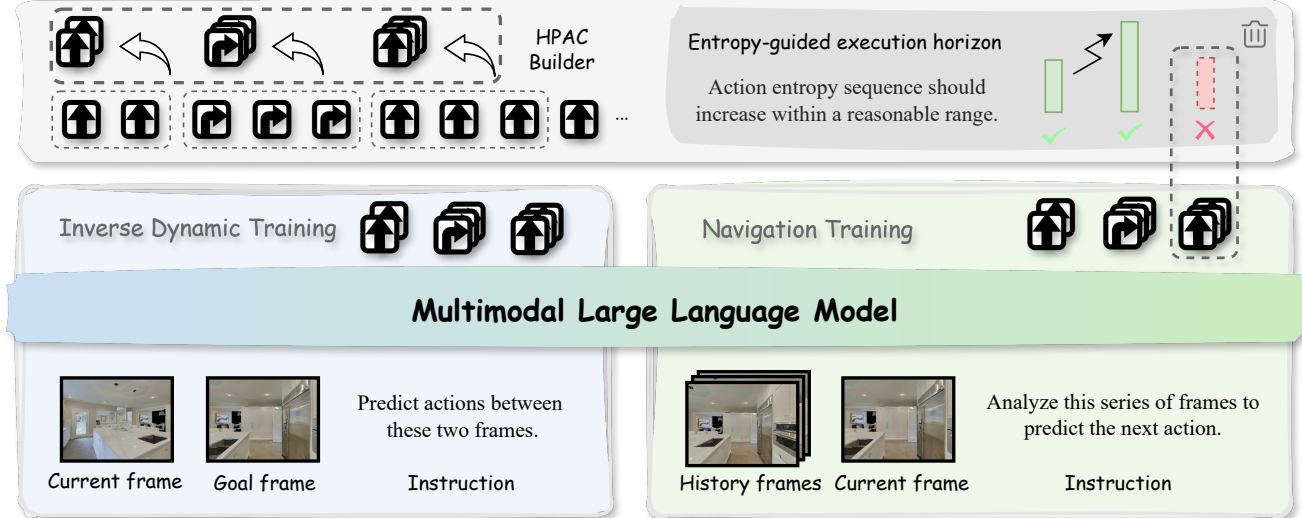


Figure 2. Architecture of NAVIDA. A multimodal language-model backbone outputs HPAC action blocks; training jointly optimizes navigation and IDM to strengthen the causal link between visual change and action, while inference uses entropy-guided execution horizon truncation to limit error accumulation.

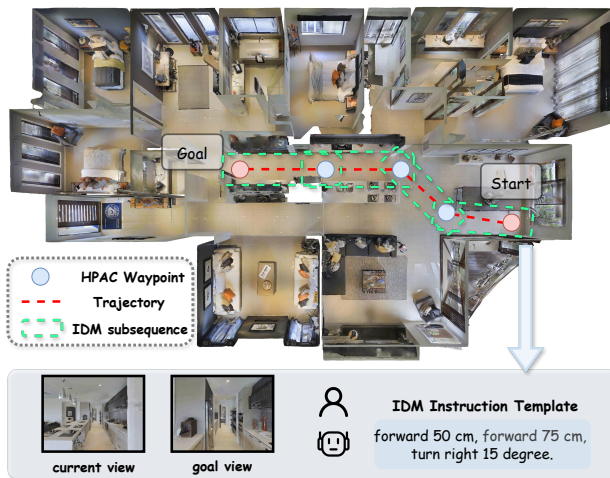


Figure 3. IDM data construction pipeline. From Habitat trajectories, HPAC groups atomic actions into variable-length blocks and induces waypoints; start-end frames yield (current, goal) views, and the intervening actions are ground-truth labels.

the goal view, and the intervening action chunk as the label (Fig. 3). This yields approximately 2.4M IDS triplets and an additional  $\sim 2.8$ M chunked VLN samples built under the same grammar.

During training, we jointly optimize the IDS and VLN objectives with shared parameters and task-specific prompts. For IDS, the model predicts  $y_t$  from  $(v_t, v_{t+\ell})$  under a task-agnostic prompt  $\mathcal{I}_{\text{IDS}}$ ,

$$\mathcal{L}_{\text{IDS}}^{\tau} = - \sum_t \sum_{j=1}^{n_t} \log p(y_{t,j}^* \mid y_{t,<j}^*, \mathcal{I}_{\text{IDS}}, v_t, v_{t+\ell}), \quad (1)$$

while for VLN the model predicts the next chunk from the visual history and instruction,

$$\mathcal{L}_{\text{VLN}}^{\tau} = - \sum_t \sum_{j=1}^{n_t} \log p(y_{t,j}^* \mid y_{t,<j}^*, \mathcal{I}_{\text{NAV}}, v_{<t}). \quad (2)$$

The combined objective  $\mathcal{L} = \sum_{\tau \in D} (\mathcal{L}_{\text{VLN}}^{\tau} + \mathcal{L}_{\text{IDS}}^{\tau})$  regularizes the representation to agree between actions that cause observed transitions and actions decoded under instructions, preserving the VLN action space and avoiding prediction of high-dimensional future appearance. With a unified chunk representation in place, inference can further exploit chunk-level uncertainty, which motivates the entropy-guided execution strategy described next.

### 3.4. Entropy-Guided Execution Horizon.

In multi-step decoding, executing the entire predicted sequence hampers responsiveness and accumulates errors, whereas executing too short a prefix may induce discontinuities and mode switching [5, 32]. To balance these effects, we leverage entropy as an uncertainty measure to assess the model’s confidence during action generation, and use it to adaptively truncate the execution horizon.

We calculate the action entropy of the model during inference. We ignore numeric tokens and focus solely on those representing action types, since once an action type is determined, the range of possible numerical tokens becomes highly constrained, and the choice of action type typically plays a more decisive role in navigation behavior at critical decision points. As is shown in Eq. (3),  $N$  represents the number of action type tokens,  $\mathcal{V}$  is the vocabulary

Table 1. Comparison with state-of-the-art methods on VLN-CE R2R Val-Unseen split. Observations used include panoramic view (Pano.), odometry (Odo.), depth sensor (Depth) and single RGB camera (S.RGB). All results are from their respective papers. \*indicates methods using the waypoint predictor. Best results are highlighted in bold, and the second results are underlined.

Method	Venue	VLM # Params	Observation				R2R Val-Unseen			
			Pano.	Odo.	Depth	S.RGB	NE $\downarrow$	OS $\uparrow$	SR $\uparrow$	SPL $\uparrow$
HPN+DN* [19]	ICCV2021	-	✓	✓	✓		6.31	40.0	36.0	34.0
CMA* [15]	CVPR2022	-	✓	✓	✓		6.20	52.0	41.0	36.0
VLN $\circ$ BERT* [15]	CVPR2022	-	✓	✓	✓		5.74	53.0	44.0	39.0
Sim2Sim* [17]	ECCV2022	-	✓	✓	✓		6.07	52.0	43.0	36.0
GridMM* [36]	ICCV2023	-	✓	✓	✓		5.11	61.0	49.0	41.0
ETPNav* [2]	TPAMI2024	-	✓	✓	✓		4.71	65.0	57.0	49.0
ScaleVLN* [35]	ICCV2023	-	✓	✓	✓		4.80	—	55.0	51.0
InstructNav [24]	CoRL2024	-	-	-	-	-	6.89	—	31.0	24.0
LAW [26]	EMNLP2021	-		✓	✓	✓	6.83	44.0	35.0	31.0
CM2 [13]	CVPR2022	-		✓	✓	✓	7.02	41.5	34.3	27.6
ETPNav + FF [38]	CoRL2024	-		✓	✓	✓	5.95	55.8	44.9	30.4
Seq2Seq [18]	ECCV2020	-			✓	✓	7.77	37.0	25.0	22.0
NavMorph [42]	ICCV2025	-			✓	✓	5.75	56.9	47.9	33.2
NaVid [44]	RSS2024	7B				✓	5.47	49.1	37.4	35.9
NaVILA [8]	RSS2025	8B				✓	5.22	62.5	54.0	49.0
UniNaVid [46]	RSS2025	7B				✓	5.58	53.3	47.0	42.7
Aux-Think [33]	NeurIPS2025	8B				✓	6.08	60.0	54.8	46.9
StreamVLN [39]	arXiv2507	7B				✓	4.98	64.2	56.9	51.9
MonoDream [34]	arXiv2508	2B				✓	5.45	61.5	55.8	49.1
InternVLA-N1(S2) [10]	-	7B				✓	4.89	60.6	55.4	52.1
InternVLA-N1(S1+S2) [10]	-	8B				✓	4.83	63.3	58.2	54.0
NavFoM [45]	arXiv2509	7B				✓	5.01	64.9	56.2	51.2
JanusVLN [43]	arXiv2509	8B				✓	4.78	65.2	60.5	<b>56.8</b>
NAVIDA (ours)	-	3B				✓	<b>4.32</b>	<b>69.5</b>	<b>61.4</b>	<u>54.7</u>

and  $p_i^v$  is the probability of the token  $v$  at time  $i$ .

$$H_t = - \sum_{i=1}^N \sum_{v \in \mathcal{V}} p_i^v \log p_i^v. \quad (3)$$

We assume that the entropy of predicted actions should monotonically increase with the prediction horizon, reflecting the growing uncertainty of actions farther into the future. Conversely, a sudden entropy drop indicates inconsistency or overconfidence in the model’s long-horizon predictions. Since the final predicted action block typically corresponds to a distant and less reliable step, it is discarded. The sequence is truncated once the action entropy ceases to increase, ensuring that only the preceding action blocks with a consistent rising entropy trend are executed.

Formally, given a predicted action chunk list  $\{a_1, a_2, \dots, a_T\}$  and their corresponding entropies  $\{H_1, H_2, \dots, H_T\}$ , the executed subset is defined as:

$$t^* = \begin{cases} \min\{t \mid H_t > H_{t+1}\}, & \text{if } \exists t \text{ s.t. } H_t > H_{t+1}, \\ T-1, & \text{otherwise.} \end{cases}$$

$$\mathcal{A}_{\text{exec}} = \{a_1, a_2, \dots, a_{t^*}\}. \quad (4)$$

## 4. Experiment

### 4.1. Experiments Setup

**Implementation Details.** We implement NAVIDA on top of Qwen-2.5-VL-3B [4]. During training, the vision encoder is frozen, while the projector and LLM backbone are optimized with a learning rate of  $2e-5$  for one epoch over mixed VLN and inverse-dynamics data. Following NaVILA [8], we cap the temporal context at eight historical frames; if a sequence exceeds this limit, we uniformly sub-sample it to eight frames to preserve coverage across the full trajectory. Unless otherwise stated, HPAC uses merge probability  $p = 0.7$  and a maximum level-2 chunk size of  $n = 3$ . At inference, we apply entropy-guided execution, which adaptively truncates the decoded chunk list to prevent long-horizon drift. Further hyperparameter details are provided in the Supplementary Material.

**Evaluation Benchmarks.** We evaluate NAVIDA on VLN-CE using the val-unseen splits of R2R-CE [3, 18] and RxR-CE [18, 20]. Following standard practice [10, 33, 43], we report Navigation Error (NE), Success Rate (SR), Oracle Success rate (OS), Success weighted by Path Length (SPL) and normalized Dynamic Time Warping (nDTW). These metrics jointly capture goal completion, trajectory efficiency, and path fidelity, and allow direct comparison to recent RGB-only and multi-sensor approaches. Detailed

Table 2. Comparison with state-of-the-art methods on VLN-CE RxR Val-Unseen split. Observations used include panoramic view (Pano.), odometry (Odo.), depth sensor (Depth) and single RGB camera (S.RGB). All results are from their respective papers. Best results are highlighted in bold, and the second results are underlined.

Method	Venue	VLM # Params	Observation				RxR Val-Unseen			
			Pano.	Odo.	Depth	S.RGB	NE $\downarrow$	SR $\uparrow$	SPL $\uparrow$	nDTW $\uparrow$
NaVILA [8]	RSS2025	8B				✓	6.77	49.3	44.0	58.8
UniNaVid [46]	RSS2025	7B				✓	6.24	48.7	40.9	-
Aux-Think [33]	NeurIPS2025	8B				✓	6.24	52.2	40.2	-
StreamVLN [39]	arXiv2507	7B				✓	6.22	52.9	46.0	61.9
MonoDream [34]	arXiv2508	2B				✓	6.38	49.4	40.9	-
InternVLA-N1(S2) [10]	-	7B				✓	6.41	49.5	41.8	62.6
InternVLA-N1(S1+S2) [10]	-	8B				✓	5.91	53.5	46.1	<u>65.3</u>
NavFoM [45]	arXiv2509	7B				✓	<u>5.51</u>	<b>57.4</b>	<u>49.4</u>	60.2
JanusVLN [43]	arXiv2509	8B				✓	6.06	<u>56.2</u>	47.5	62.1
NAVIDA (ours)	-	3B				✓	<b>5.23</b>	<b>57.4</b>	<b>49.6</b>	<b>67.0</b>



Figure 4. Qualitative results of NAVIDA on VLN-CE R2R Val-Unseen split. Correct actions are marked with green arrows, while incorrect actions are marked with red arrows.

explanations of the metrics are provided in the Supplementary Material.

**Real-World Evaluation Setup.** In real-world experiments, we employ two humanoid robot platforms, the AgiBot X2 and the Unitree G1, in an indoor working environment. The AgiBot X2 is equipped with two monocular fisheye RGB cameras; we used only one of them and converted it into an image equivalent to that captured by a pinhole camera. For the Unitree G1, its built-in camera is downward-mounted, and its  $55.2^\circ$  field of view (FOV) cannot cover the area directly in front of the robot. Therefore, we addi-

tionally mounted a RealSense D455f camera on its chest. When the robot receives a command, it uploads the current RGB image to NAVIDA deployed on a remote server equipped with an NVIDIA 4090 GPU. NAVIDA outputs the action sequence in 0.93 seconds. After receiving the action command from the server, the robot executes the command through the robot's motion API.

## 4.2. Main Results

**Performance Evaluation.** As shown in Tab. 1 (R2R-CE) and Tab. 2 (RxR-CE), NAVIDA delivers state-of-the-art results on the val-unseen splits while using only a



You are now facing the sofa. Turn left, then right near the refrigerator, and continue walking straight down the path until you stop at the first row of wo...



Turn right out of the bedroom, then walk straight along the main path in the hall and stop to the left of the first wooden door.



Turn right, walk straight ahead, enter the first room in front of you, and stop when you see the table.

Figure 5. Real world results of NAVIDA. The robot’s direction of motion is indicated by arrows in the diagram.

single RGB stream and a 3B backbone VLM. On R2R-CE, NAVIDA attains the best NE/OS/SR and the second-best SPL, surpassing the strongest RGB-only 8B baseline JanusVLN [43] by -0.46 NE, +4.3 OS, and +0.9 SR. These gains demonstrate that modeling action-vision causality improves goal attainment without sacrificing path efficiency. On RxR-CE, NAVIDA matches the best SR (57.4) and achieves the best NE/SPL/nDTW, improving over StreamVLN [39] and JanusVLN by +1.2 to +4.5 SR, +2.1 to +3.6 SPL, and -0.83 to -0.99 NE. The consistent advantage on the linguistically richer, longer-horizon RxR-CE indicates stronger long-range alignment and reduced drift, attributable to IDS and hierarchical chunking.

Compared with multi-sensor (e.g., ETPNav [2] and NavMorph [42]), NAVIDA’s single-RGB policy still leads on core metrics in both benchmarks, despite several competitors using panoramic RGB, depth, or odometry. Moreover, compared with other single RGB input methods, NAVIDA achieves the best results with 35% of the parameters and without auxiliary generators or spatial encoders. This further highlights the efficiency of action-grounded supervision as a training paradigm rather than a capacity increase. In summary, NAVIDA consistently outperforms strong RGB-only baselines and methods with richer sensors, establishing that inverse-dynamics augmentation plus HPAC forms an effective and lightweight alternative to conventional map/history cues and forward world modeling.

**Qualitative Results.** Fig. 4 contrasts NAVIDA with a variant without IDS where green arrows mark correct actions and red arrows mark errors. NAVIDA correctly defers turn-

Table 3. Ablation study of IDS on VLN-CE R2R Val-Unseen split. We denote training *without* IDS by  $\circ$ , and *with* IDS by  $\bullet$ . Blank cells indicate the dataset is not used.

R2R	RxR	DAgger	NE $\downarrow$	OS $\uparrow$	SR $\uparrow$	SPL $\uparrow$
$\circ$			7.86	44.5	32.0	27.6
$\bullet$			6.99	51.5	40.5	35.5
$\bullet$	$\bullet$		5.72	57.4	47.7	41.5
$\bullet$	$\bullet$	$\circ$	5.25	60.9	53.7	47.0
$\circ$	$\circ$	$\circ$	5.29	61.9	52.6	47.1
$\bullet$	$\bullet$	$\bullet$	<b>4.91</b>	<b>63.2</b>	<b>55.5</b>	<b>49.6</b>

ing until clearing the staircase and selects the intended intersection, whereas the ablated model exhibits premature turns and junction misclassification. These are typical symptoms of error accumulation when future visual consequences of actions are not internalized.

Fig. 5 presents examples of real-world trials. NAVIDA executes tight turns at narrow corners and passes smoothly through single-person doorways; even with pedestrians ahead, it resists interference and holds a reliable heading. Taken together, the simulator and real-world evidence identify IDS as the key component behind the observed stability and scene generalization, outperforming the variant without inverse-dynamics supervision.

### 4.3. Ablation Study

In this section, we conduct ablations on the effectiveness of IDS, the length of HPAC, entropy-based execution horizon selection and dynamic modeling methods. To ensure effi-

ciency, we conduct experiments on data without ScaleVLN and report the performance on R2R-CE benchmark. We do not use entropy-based execution horizon selection mechanism by default unless otherwise stated.

**Effect of IDS Data.** Tab. 3 varies whether R2R, RxR, and DAgger trajectories contribute IDS pairs (●) or not (○). Using IDS consistently improves all metrics: on R2R alone, SR rises from 32.0 to 40.5; with R2R+RxR, SR increases to 47.7; adding DAgger without IDS yields SR 52.6, while enabling IDS across all three reaches SR 55.5 with lower NE (4.91) and higher SPL (49.6). The performance gains are most pronounced in data-scarce scenarios and continue to accumulate as additional data sources are introduced. This pattern suggests IDS injects a transferable, language-agnostic notion of “how actions change what is seen,” which complements imitation rollouts such as DAgger.

**Ablations of the Chunk Number.** Table 4 shows the impact of the maximum number of action chunks allowed in HPAC on the VLN-CE R2R Val-Unseen split. When the maximum number of action chunks is equal to 1, we set the merging probability to 1 to make it equivalent to the action merging method used in previous works. We found that optimal performance was achieved when the model was allowed to output 3 action chunks at a time, while fewer or more chunks resulted in degraded performance. We believe that appropriately increasing the number of action chunks predicted by the model can improve its long-term path planning capabilities, while predicting too many action chunks would exceed its perception limit, leading to suboptimal action predictions due to a lack of global knowledge.

Table 4. Ablation study of the maximum chunk number in HPAC on VLN-CE R2R Val-Unseen split.

Max Chunk Number	NE↓	OS↑	SR↑	SPL↑
1	5.08	62.2	54.4	48.8
2	4.94	60.8	54.2	48.9
3	<b>4.91</b>	<b>63.2</b>	<b>55.5</b>	<b>49.6</b>
4	5.23	60.2	52.5	46.4

**Entropy-Based vs. Fixed Execution Horizon.** Tab. 5 presents our ablation study of entropy-based action execution horizon selection. As a comparison, we truncate the action chunks after a fixed number of action chunks. It can be seen that selecting an appropriate execution horizon (the second row) effectively improves the model’s performance in unseen scenarios. Furthermore, the action entropy-based execution horizon selection method is more effective than fixed-size execution horizon selection, demonstrating the benefit of adapting to the model’s uncertainty dynamics.

**Inverse vs. Forward Dynamics.** To evaluate the effectiveness of inverse dynamics supervision, we compared it with forward dynamics supervision (FDS). Specifically, we follow MonoDream [34] and use a VLM to predict the visual

Table 5. Ablation study of the execution horizon on VLN-CE R2R Val-Unseen split.

Execution Horizon Method	NE↓	OS↑	SR↑	SPL↑
Truncated@chunk 1	5.09	62.9	55.5	49.3
Truncated@chunk 2	4.93	63.3	56.2	50.4
Truncated@chunk 3	4.91	63.2	55.5	49.6
Entropy-based selection	<b>4.70</b>	<b>64.5</b>	<b>57.4</b>	<b>51.2</b>

features of the future without introducing any additional modules. For fairness, both methods were trained with the same amount of dynamics data for one epoch. As shown in Tab. 6, inverse dynamics supervision consistently outperforms forward dynamics supervision and the baseline model without any dynamic supervision, while forward dynamics supervision introduces significant performance degradation. We believe this difference stems from the consistency of the output space: enabling a pre-trained VLM to predict dense future visual features is typically harder to optimize and demands significant additional computation and data—for instance, MonoDream [34] requires training for five epochs. In contrast, inverse dynamics supervision aligns with the pre-training objective of the VLM, simplifying the learning of the causal relationship between visual changes and corresponding actions.

Table 6. Ablation study of the dynamic modeling on VLN-CE R2R Val-Unseen split.

Dynamic Method	NE↓	OS↑	SR↑	SPL↑
Base	5.29	61.9	52.6	47.1
w/ FDS	5.78	56.4	46.5	41.6
w/ IDS	<b>4.91</b>	<b>63.2</b>	<b>55.5</b>	<b>49.6</b>

## 5. Conclusion

In this work, we presented NAVIDA, a unified VLN framework that integrates policy learning with action-grounded visual dynamics and adaptive execution. Through chunk-based inverse-dynamics supervision, NAVIDA learns the causal relationship between visual transitions and corresponding actions, enabling more interpretable and stable navigation. The proposed hierarchical probabilistic action chunking mechanism structures navigation trajectories into multi-level motion units, providing richer and longer-range supervision for inverse dynamics learning. During inference, an entropy-guided adaptive execution mechanism dynamically adjusts the action horizon to prevent error accumulation and enhance behavioral stability. Extensive experiments demonstrate that NAVIDA achieves superior navigation performance with fewer parameters compared to state-of-the-art methods, and real-world robot evaluations confirm its effectiveness and practical applicability.

# NAVIDA: Vision-Language Navigation with Inverse Dynamics Augmentation

## Supplementary Material

### Table of Contents

<b>6. Prompts for Different Tasks</b>	<b>1</b>
<b>7. More Implementation Details</b>	<b>1</b>
7.1 . Data Details . . . . .	1
7.2 . Training Hyperparameters . . . . .	1
7.3 . Evaluation Metrics Details . . . . .	2
7.4 . Real-World Deployment Details . . . . .	3
<b>8. More Experiment Results</b>	<b>3</b>
8.1 . More Ablations . . . . .	3
8.2 . More Qualitative Results . . . . .	5

### 6. Prompts for Different Tasks

We use task-specific prompts for VLN and for inverse-dynamics supervision, both expressed in the same action grammar (action-type + numeric tokens).

For vision-language navigation task, we use the following prompt template to instruct the model to predict the corresponding action chunks:

Imagine you are a robot programmed for navigation tasks. You have been given a video of historical observations: <image>,...,<image> and current observation: <image>. Your assigned task is: [Instruction]. Analyze this series of images to decide your next move, which could involve turning left or right by a specific degree, moving forward a certain distance.

Among them, [Instruction] is the language instruction given for the current navigation task. For inverse-dynamics supervision, we use prompt a prompt template like the following:

Imagine you are a robot programmed for navigation tasks. You have been given an image of current view <image> and an image of the goal view <image>. Analyze the two images to predict the navigation action that would move the robot from the current viewpoint to the goal view, which could involve turning left or right by a specific degree or moving forward a certain distance.

For the forward-dynamics supervision in Sec. 4.3, the requirement is to predict the visual observation features of

the next time step based on the given historical frames and language instructions. We use the following prompt:

Imagine you are a robot programmed for navigation tasks. You have been given a video of historical observations: <image>,...,<image> and current observation: <image>. Your assigned task is: [Instruction]. Analyze this series of images to predict the future observation.

### 7. More Implementation Details

#### 7.1. Data Details

Fig. 6 depicts the distribution of atomic actions per HPAC chunk in our inverse-dynamics (IDM) dataset. The majority of chunks contain 3 to 5 atomic actions, consistent with the fixed chunk sizes used in prior works [8, 39, 44], while a smaller number of samples contain either fewer or more atomic actions. Longer chunks encode larger egocentric viewpoint shifts and parallax, yielding strong, informative supervision signals for inverse dynamics and supporting long-horizon planning by offering the model an extended temporal context. In contrast, shorter chunks emphasize subtle, fine-grained visual changes (e.g., small turns or local re-alignments), which facilitate precise control and reduce action ambiguity at short horizons. This natural mixture of long and short chunks serves as a complementary curriculum: HPAC contributes global structural cues for planning alongside local adjustment priors for stabilization, thereby strengthening the causal grounding between visual observations and actions and improving robustness to compounding errors during execution.

We also normalized the navigation process to a range of 0 to 1, and Fig. 7 shows the distribution of action chunks as the navigation process progresses. It can be seen that in the early stages of navigation, HPAC merges a large number of atomic actions, which decreases slightly and stabilizes in the middle stages. In the later stages of navigation, closer to the target, HPAC tends to use fewer atomic actions to stabilize the robot’s position.

#### 7.2. Training Hyperparameters

NAVIDA is implemented on Qwen-2.5-VL-3B; the vision encoder is frozen and only the projector and LLM are trainable. We use AdamW with  $lr = 2e-5$ , BF16, Flash-Attention v2, global batch size = 64; additional hyperparameters are summarized in Tab. 7.

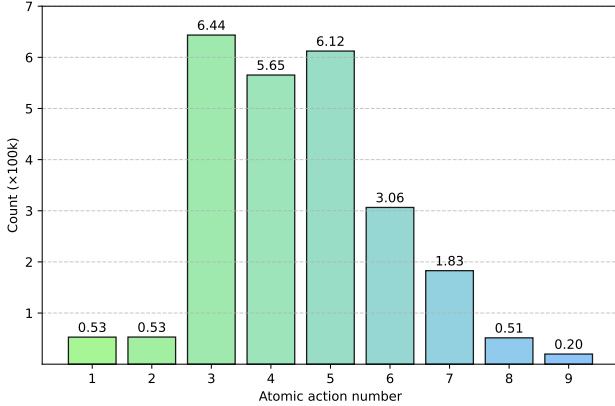


Figure 6. Distribution of atomic actions per HPAC chunk in the IDM data. Most chunks contain 3–5 atomic actions.

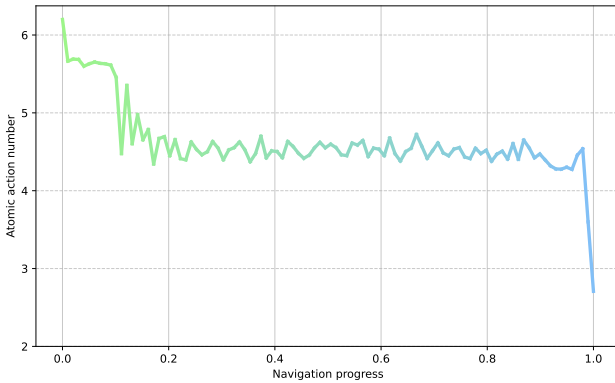


Figure 7. Distribution of actions on navigation progress.

Table 7. Training hyperparameters used for fine-tuning Qwen2.5-VL. Only the projector and LLM modules are trainable.

Hyperparameter	Value
Training epochs	1
Trainable modules	Projector + LLM
Learning rate	$2e - 5$
Optimizer	AdamW
AdamW $\beta_1$	0.9
AdamW $\beta_2$	0.999
Adam $\epsilon$	$1e - 8$
Lr schedule	Linear
Global batch size	64
Gradient accumulation	4
Mixed precision type	BFloat16
Attention type	Flash Attention v2
LLM sequence length	64800
Image resolution	$308 \times 252$

### 7.3. Evaluation Metrics Details

To formalize the evaluation criteria and relate each metric to its practical intuition, we report Navigation Error (NE), Success Rate (SR), Oracle Success Rate (OSR), Success-weighted Path Length (SPL), and normalized Dynamic Time Warping (nDTW). In brief, lower is better for NE; higher is better for SR/OSR/SPL/nDTW.

**Navigation Error (NE).** NE measures the final distance between the agent’s stopping position  $\mathbf{p}_T$  and the goal location  $\mathbf{g}$ . It is defined as:

$$NE = d(\mathbf{p}_T, \mathbf{g}), \quad (5)$$

where  $d(\cdot, \cdot)$  denotes the geodesic distance in the navigation environment. Smaller NE indicates better terminal accuracy.

**Success Rate (SR).** A navigation episode is considered successful if the agent stops within a threshold distance  $\tau$  from the goal. The success rate is defined as:

$$SR = \frac{1}{N} \sum_{i=1}^N \mathbf{1}[d(\mathbf{p}_T^{(i)}, \mathbf{g}^{(i)}) \leq \tau], \quad (6)$$

where  $N$  is the total number of episodes and  $\tau$  is set to 3 in most VLN settings. Higher SR reflects more consistent goal completion.

**Oracle Success Rate (OSR).** OSR evaluates whether the agent was ever within the success radius  $\tau$  during its entire trajectory, regardless of its final stop:

$$OSR = \frac{1}{N} \sum_{i=1}^N \mathbf{1}\left[\min_t d(\mathbf{p}_t^{(i)}, \mathbf{g}^{(i)}) \leq \tau\right]. \quad (7)$$

where  $\mathbf{p}_t^{(i)}$  is the  $t$ -th position of the robot in the  $i$ -th episode. OSR is informative for understanding recoverability and premature stopping.

**Success-weighted Path Length (SPL).** SPL measures the efficiency of successful navigation, comparing the shortest geodesic path length  $L^{(i)}$  with the agent’s actual traversed path length  $P^{(i)}$ :

$$SPL = \frac{1}{N} \sum_{i=1}^N \mathbf{1}[d(\mathbf{p}_T^{(i)}, \mathbf{g}^{(i)}) \leq \tau] \cdot \frac{L^{(i)}}{\max(P^{(i)}, L^{(i)})}. \quad (8)$$

SPL is 0 for failures (via the indicator) and approaches 1 when successful paths are near-optimal.

**Normalized Dynamic Time Warping (nDTW).** nDTW measures the trajectory similarity between the agent path  $\{\mathbf{p}_t\}_{t=1}^T$  and the shortest-path reference trajectory  $\{\mathbf{q}_k\}_{k=1}^K$  using dynamic time warping distance  $DTW(\cdot, \cdot)$ :

$$nDTW = \exp\left(-\frac{DTW(\mathbf{p}_{1:T}, \mathbf{q}_{1:K})}{\eta}\right), \quad (9)$$

where  $\eta$  is a normalization constant (typically the shortest-path length). This exponential normalization converts the alignment cost into a bounded similarity score within the range  $(0, 1]$ , where values closer to 1 indicate higher spatial and temporal consistency with the optimal reference trajectory. Intuitively, nDTW rewards trajectories that closely follow the correct route, even if their timing or step correspondence differs slightly. Compared to simple geometric distance metrics, nDTW provides a more flexible and robust measure of path-following quality, as it accounts for local temporal misalignments and route overlaps that commonly occur during navigation.

#### 7.4. Real-World Deployment Details

Fig. 8 shows the overall architecture of our real-world deployment system. Specifically, NAVIDA was deployed on a remote computation server equipped with an NVIDIA RTX 4090 GPU. The system follows a client–server structure, where the robot functions as the client that collects sensory data and executes movement commands, while the remote server is responsible for high-level reasoning and action prediction.

During operation, the robot continuously captures RGB images from its front-facing camera (as shown in Fig. 9) and receives natural language or voice commands from the user through a local area network. The sensory data and corresponding commands are then packaged and transmitted to the remote server via the internet. On the server side, the NAVIDA model processes these inputs, performs vision-language reasoning, and predicts the next navigation action. The predicted motion command is then sent back to the robot, where it is converted into executable parameters such as linear velocity, angular velocity, and movement duration through the robot’s motion control API.

In addition, we provide demonstration videos of real-world deployment, which are submitted together with the supplementary materials. The slight latency observed in the videos mainly results from **network communication delays** between the robot and the remote server.

Table 8. Ablation study of the vision encoder fine-Tuning on VLN-CE R2R Val-Unseen split.

Vision Encoder	NE $\downarrow$	OS $\uparrow$	SR $\uparrow$	SPL $\uparrow$
Trainable	5.12	<b>63.6</b>	<b>55.6</b>	49.2
Frozen	<b>4.91</b>	63.2	55.5	<b>49.6</b>

## 8. More Experiment Results

### 8.1. More Ablations

**Data Scale.** Fig. 11 illustrates the performance trend of NAVIDA on R2R-CE Val-Unseen as a function of the

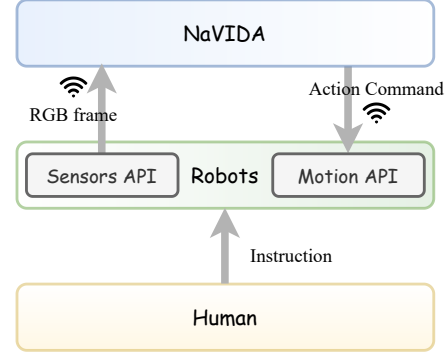


Figure 8. Architecture of the deployed system used for real-world evaluation. RGB frames and user instructions are transmitted from the robot to a remote server running NAVIDA, which predicts action sequences and returns motion commands for execution through the robot’s motion API.

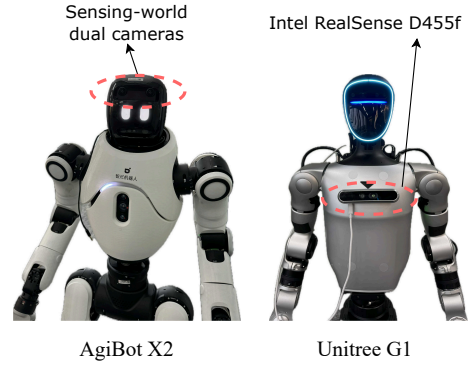


Figure 9. Robot platforms and sensing configuration. AgiBot X2 (left) equipped with a single rectified fisheye RGB camera and Unitree G1 (right) with an additional Intel RealSense D455f front-facing camera, providing consistent monocular RGB input for NAVIDA’s navigation policy.

total data size, which includes both IDS and VLN data. As the total data size increases, NAVIDA consistently achieves better performance. The improvement is particularly pronounced when the data scale is small, indicating that NAVIDA effectively leverages additional data to learn more robust representations in low-data regimes. However, as the total data scale continues to grow, the performance gains gradually saturate. This behavior likely reflects a diminishing returns effect, where the model has already captured most of the useful patterns from the available data, and further increases in data size contribute less to performance. Additionally, the stabilization may indicate that other factors such as model capacity, task complexity, or inherent noise in the data become the limiting factors once a certain data threshold is reached.

**Vision Encoder: Frozen vs. Trainable.** We conduct an ablation study to evaluate the impact of fine-tuning the vision encoder on overall navigation performance. As shown

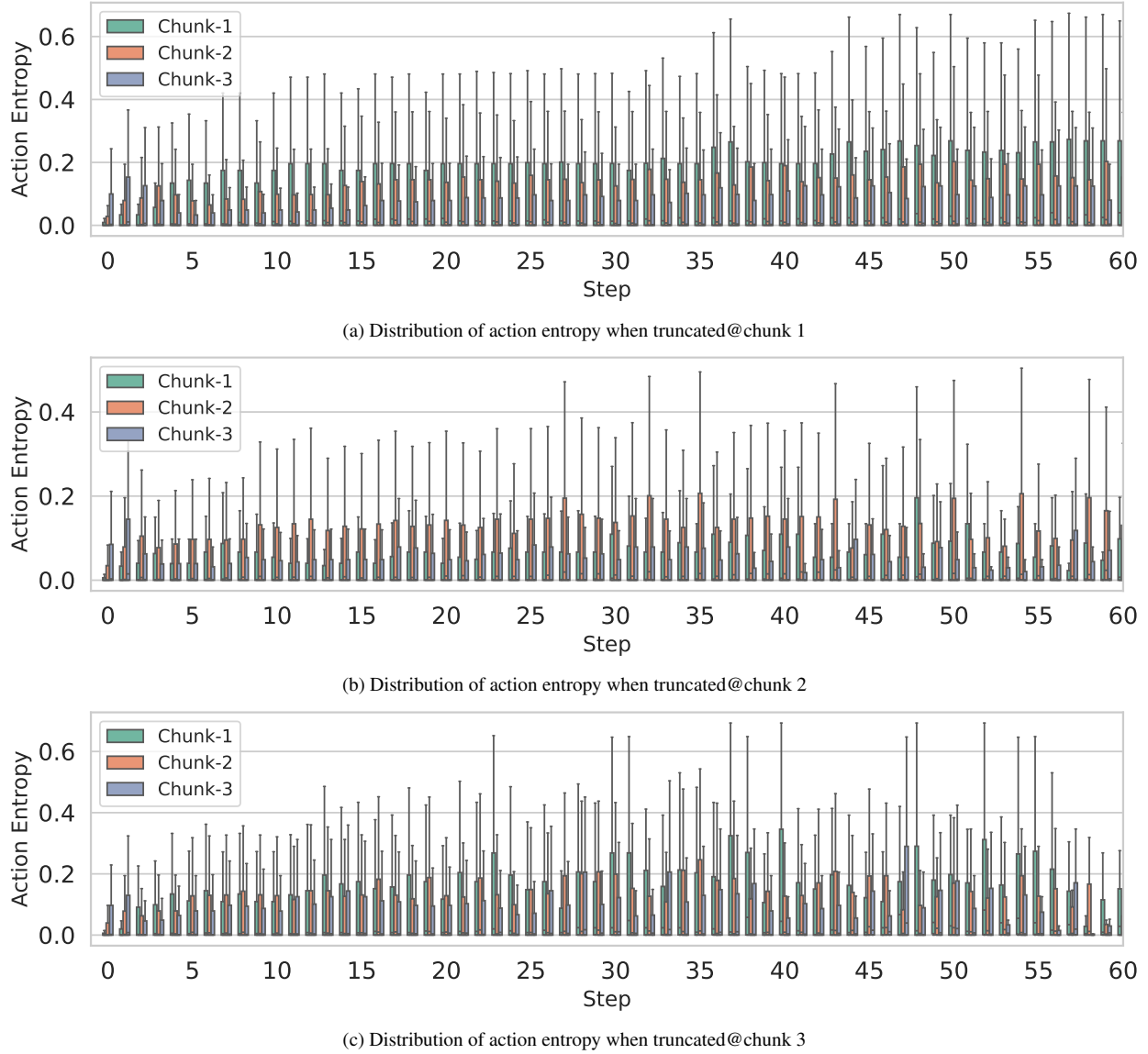


Figure 10. Action-type entropy across decoding steps under fixed truncation@chunk 1,2,3. Entropy is computed over action-type tokens only. In theory it should increase with horizon; a local drop signals unreliable long-range predictions, motivating truncation before the drop and yielding a more stable executed prefix.

in Tab. 8, unfreezing the vision encoder and training it end-to-end provides only marginal improvements compared to keeping it frozen. This result suggests that the pre-trained visual representations are already sufficiently informative for downstream navigation tasks, and further adaptation offers limited benefit. Moreover, fine-tuning substantially increases GPU memory usage and training time, with minimal returns in accuracy. Therefore, we keep the vision encoder frozen in all subsequent experiments, enabling the model to efficiently utilize robust pre-trained visual features while maintaining a favorable balance between performance and computational efficiency.

**Number of History Frames.** We perform an ablation study to investigate how the number of historical frames influences navigation performance on the R2R-CE Val-Unseen split. All models are trained solely on the R2R training data for consistency. As shown in Tab. 9, using 8 history frames is sufficient to capture most instruction horizons, providing the model with adequate temporal context for action reasoning. Increasing the number of frames to 16 does not yield noticeable performance gains and occasionally leads to a slight degradation, likely due to redundant or noisy visual information accumulated over longer sequences. This behavior aligns with findings from NaVILA [8], indicating

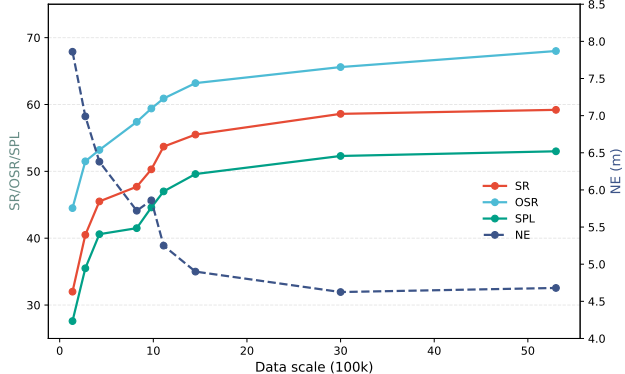


Figure 11. Navigation performance of NAVIDA on VLN-CE R2R Val-Unseen split with the increase of data scale. SR/OSR/SPL increase and NE decreases as data grows, with gains tapering at larger scales.

that excessive historical context can dilute the relevance of recent observations and hinder temporal grounding. Hence, we adopt 8 history frames as a balanced choice between contextual richness and model efficiency.

Table 9. Ablation study of the number of history frames on VLN-CE R2R Val-Unseen split.

# History Frames	NE $\downarrow$	OS $\uparrow$	SR $\uparrow$	SPL $\uparrow$
8	<b>6.99</b>	<b>51.5</b>	<b>40.5</b>	35.5
16	7.02	50.1	40.4	<b>36.1</b>

**Inverse vs. Forward Dynamics.** Considering the slower convergence of Forward Dynamics Supervision (FDS), we conducted extended training to further compare its effectiveness and efficiency against Inverse Dynamics Supervision (IDS). Specifically, FDS was trained for a total of 3 epochs, with checkpoints saved after each epoch for evaluation. As shown in Tab. 10, the performance of FDS gradually improves with additional training epochs, eventually surpassing the baseline model without any dynamic supervision at the third epoch. However, even after prolonged training, FDS still underperforms compared to IDS, which achieves superior results after only a single epoch. This observation highlights that IDS provides more stable and data-efficient supervision signals by directly modeling the causal relationship between consecutive observations and actions. In contrast, FDS requires longer optimization to learn reliable predictive mappings for future states. Overall, these findings underscore the superior training efficiency and effectiveness of IDS in enhancing visual-language navigation performance.

**Action Entropy** Fig. 10 shows action-entropy distributions under different fixed truncation policies for the execution horizon. We compute action entropy at step  $t$ , which serves as a proxy for behavioral uncertainty: high  $H_t$  indicates the

Table 10. Ablation study of the dynamic modeling on VLN-CE R2R Val-Unseen split.

Dynamic Method	NE $\downarrow$	OS $\uparrow$	SR $\uparrow$	SPL $\uparrow$
Base	5.29	61.9	52.6	47.1
w/ FDS (epoch-1)	6.13	56.0	44.6	38.7
w/ FDS (epoch-2)	5.06	60.1	51.0	45.2
w/ FDS (epoch-3)	5.06	62.4	53.9	48.2
w/ IDS	<b>4.91</b>	<b>63.2</b>	<b>55.5</b>	<b>49.6</b>

policy is uncertain about which action type to choose, while low  $H_t$  indicates confident selection.

In sequential prediction, a gradual increase of  $H_t$  with horizon is expected, because uncertainty compounds as visual evidence becomes less informative and small pose errors accumulate. Occasionally, however, we observe local decreases of entropy in later chunks during inference. Such entropy dips often reflect spurious overconfidence induced by dataset bias rather than genuine visual or spatial reasoning. For example, after two consecutive “move forward 75 cm” actions, the training data may frequently contain a “turn right 30 degree” action, which encourages the model to snap to that action with high confidence based on co-occurrence patterns in the text space, even when current images do not support this choice. This kind of shortcut leads to low entropy that is unjustified by the scene and degrades reliability.

These observations motivate an entropy-guided execution-horizon strategy. We retain the prefix that follows the expected rising-entropy trend and truncate before the first entropy dip, that is, at the preceding local peak. Executing only up to this peak avoids high-risk segments dominated by biased priors, reduces error compounding, and improves trajectory stability. Empirically, when truncation is fixed after chunk 1 or 2, the entropy peak aligns with the chosen boundary (Figs. 10a and 10b); when truncation is disabled and all three chunks are executed, the entropy profile becomes irregular because the unreliable final chunk perturbs the distribution (Fig. 10c). This rule detects the earliest deviation from a monotonic rise and stops at the last reliable peak, balancing action completeness and reliability without additional training.

## 8.2. More Qualitative Results

We present extensive qualitative results of NAVIDA in both real-world and simulated environments to further demonstrate its effectiveness and generalization ability, as shown in Fig. 12, Fig. 13, and Fig. 14. The results show that NAVIDA produces smooth, instruction-aligned trajectories in simulation and robustly executes navigation commands in real-world settings. These findings highlight the model’s strong cross-domain generalization, accurate language grounding, and reliable decision-making in complex, long-horizon navigation tasks.



Turn right and walk along this road. At the first door, turn left and go through that door. You will then see two rows of elevator doors; that is your destination.



Turn left and keep walking straight. When you see a red billboard, turn right. You will then see a staircase entrance with signs. Stop in front of the signs.



Continue straight along the current path, turn right at the first intersection, and keep going until you see a left or right path; that's your destination.



Turn right and walk along the current road, and enter the room ahead. Stop in front of the table.

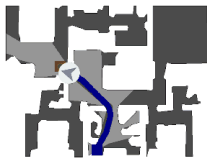


You are now facing the head of the bed in the bedroom. Turn around and walk out of the bedroom. Keep walking straight ahead and you will see a sofa. Walk closer to the sofa and turn right. After that, you will see a water dispenser and a refrigerator. Walk towards the refrigerator and stop in front of it.



Turn left, walk towards the sofa, then turn slightly right towards the cabinet with the microwave. Walk towards the door next to it, and you will enter the bedroom. You will find the bed on your right. Move closer to the bed and stop facing it.

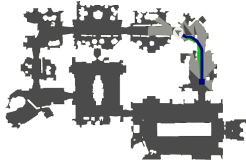
Figure 12. Qualitative results of NAVIDA on real world.



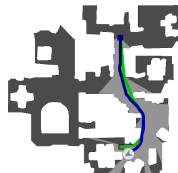
Go through the door and turn left. Go to the left of the stairs. Stop in the doorway to the left of the white double doors.



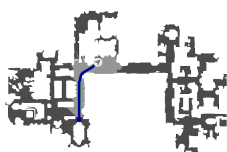
Walk out of the room and turn right. Turn right at the stairs and walk into the bed room. Turn left and take another left at the nightstand. Wait in the doorway next to the nightstand.



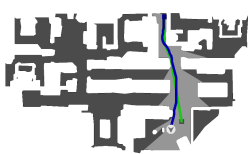
Walk past the white marble bust on a pedestal to the right. Take a left at the barricade stanchion to the left. Wait at the fire extinguisher on the floor to the left.



Walk down the hall in the direction of the stairs to the second floor. Pass the stairs and enter the living room. Take a right in the living room. Stop on the right of the chair at the head of the table.

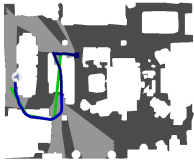


Walk down the hall to the last bar bench. Make a right into the connecting hallway, take a left at the opening of the first room.

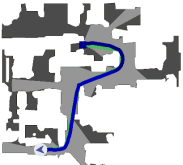


Move forward into the room, exit the room and continue straight into an eating area, continue straight into the living room, and stop right next to the rug in front of the couch.

Figure 13. Qualitative results of NAVIDA on VLN-CE R2R Val-Unseen split.



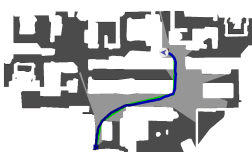
You're starting at the base of a wooden staircase. Go up these stairs. At the top of the stairs, turn right and take a step to the right of the white door that's open. Turn right and walk down this catwalk, passing the brown cabinet on your left. Go onto the rug in front of you. You should be at the foot of the twin bed on the left. Go inside the door to the left of that bed. This is a bathroom. Take two steps into the shower. The shower will be on your right, the sink will be on your left and an open door to the first bedroom you came is in front of you. You're done.



Go right from the place you are standing, and enter into the room which is in front of you, now go near the bed and turn right, you will find two open doors, now step out of the room, and go straight on the left side you will find a staircase. Now turn left you will find an open door, now enter into the room, and go straight, now turn right, and go straight, there you will find an open door, enter into the door, that will be your final destination.



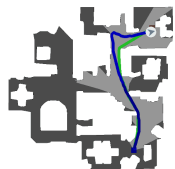
You are facing the wall. Turn slightly right and move forward, until you face the wall which has a wall hanging on it. Turn slightly left and move forward to your right, there are stairs. Climb up the stairs. At the top of the stairs, turn slightly left and move forward then you are facing towards the plants. Turn slightly right and move forward, then you are facing towards the plant. Turn slightly right and move forward until you are facing the wall again. Turn slightly right and move forward wherein there are some flower vases to your left and right. Move forward until the sofa, then turn slightly left and walk towards the bed. Now walk beside the bed and move forward, until you are facing the wall again. Turn slightly left and move forward, this is a bathroom and stop facing the bathtub and the windows, and this is your end point.



Right now you are facing towards the sofa turn slightly right and move forward towards the clock on the wall. Then turn right and move forward then turn slightly left and move forward towards the frame on the wall on the left side. Then turn left and you can see an open entrance enter through it now you are standing near the door which is closed. You have reached your destination point.



You are on the steps, slightly take left, climb the steps and move forward, turn right, you can find stairs, climb up the stairs completely, turn left, move forward, take left, walk straight, now you are facing towards the wall, turn left, you can find an open door, enter into the room, at the entrance of the room you can find your destination.



You can find a mirror in front of you, go near the mirror, slightly turn to your left and move forward, enter into the area which is right side to the staircase, to your right you can find portraits, enter into the room which is to your left, turn back, enter into the room which is in front of you, slightly turn to your left, you can find two stools in front of you, stand in between the two stools, that would be your end point.

Figure 14. Qualitative results of NAVIDA on VLN-CE RxR Val-Unseen split.

## References

[1] Dong An, Yuankai Qi, Yangguang Li, Yan Huang, Liang Wang, Tieniu Tan, and Jing Shao. Bevbert: Multimodal map pre-training for language-guided navigation. *arXiv preprint arXiv:2212.04385*, 2022. 2

[2] Dong An, Hanqing Wang, Wenguan Wang, Zun Wang, Yan Huang, Keji He, and Liang Wang. Etpnav: Evolving topological planning for vision-language navigation in continuous environments. *IEEE Transactions on Pattern Analysis and Machine Intelligence*, 2024. 5, 7

[3] Peter Anderson, Qi Wu, Damien Teney, Jake Bruce, Mark Johnson, Niko Sünderhauf, Ian Reid, Stephen Gould, and Anton Van Den Hengel. Vision-and-language navigation: Interpreting visually-grounded navigation instructions in real environments. In *Proceedings of the IEEE conference on computer vision and pattern recognition*, pages 3674–3683, 2018. 1, 3, 5

[4] Shuai Bai, Keqin Chen, Xuejing Liu, Jialin Wang, Wenbin Ge, Sibo Song, Kai Dang, Peng Wang, Shijie Wang, Jun Tang, et al. Qwen2. 5-vl technical report. *arXiv preprint arXiv:2502.13923*, 2025. 1, 5

[5] Kevin Black, Manuel Y Galliker, and Sergey Levine. Real-time execution of action chunking flow policies. *arXiv preprint arXiv:2506.07339*, 2025. 4

[6] Wenzhe Cai, Jiaqi Peng, Yuqiang Yang, Yujian Zhang, Meng Wei, Hanqing Wang, Yilun Chen, Tai Wang, and Jiangmiao Pang. Navdp: Learning sim-to-real navigation diffusion policy with privileged information guidance. *arXiv preprint arXiv:2505.08712*, 2025. 2

[7] Shizhe Chen, Pierre-Louis Guhur, Cordelia Schmid, and Ivan Laptev. History aware multimodal transformer for vision-and-language navigation. *Advances in neural information processing systems*, 34:5834–5847, 2021. 2

[8] An-Chieh Cheng, Yandong Ji, Zhaojing Yang, Xueyan Zou, Jan Kautz, Erdem Biyik, Hongxu Yin, Sifei Liu, and Xiaolong Wang. Navila: Legged robot vision-language-action model for navigation. *Robotics: Science and Systems*, 2025. 1, 2, 5, 6, 4

[9] Cheng Chi, Zhenjia Xu, Siyuan Feng, Eric Cousineau, Yilun Du, Benjamin Burchfiel, Russ Tedrake, and Shuran Song. Diffusion policy: Visuomotor policy learning via action diffusion. *The International Journal of Robotics Research*, 44 (10-11):1684–1704, 2025. 2

[10] InternNav Contributors. InternNav: InternRobotics’ open platform for building generalized navigation foundation models. <https://github.com/InternRobotics/InternNav>, 2025. 5, 6

[11] Guangzhao Dai, Jian Zhao, Yuantao Chen, Yusen Qin, Hao Zhao, Guosen Xie, Yazhou Yao, Xiangbo Shu, and Xuelong Li. Unitedvln: Generalizable gaussian splatting for continuous vision-language navigation. *arXiv preprint arXiv:2411.16053*, 2024. 2

[12] Zi-Yi Dou, Feng Gao, and Nanyun Peng. Masked path modeling for vision-and-language navigation. *arXiv preprint arXiv:2305.14268*, 2023. 2

[13] Georgios Georgakis, Karl Schmeckpeper, Karan Wanchoo, Soham Dan, Eleni Miltsaiki, Dan Roth, and Kostas Daniilidis. Cross-modal map learning for vision and language navigation. In *Proceedings of the IEEE/CVF conference on computer vision and pattern recognition*, pages 15460–15470, 2022. 5

[14] Yicong Hong, Qi Wu, Yuankai Qi, Cristian Rodriguez-Opazo, and Stephen Gould. Vln bert: A recurrent vision-and-language bert for navigation. In *Proceedings of the IEEE/CVF conference on Computer Vision and Pattern Recognition*, pages 1643–1653, 2021. 2

[15] Yicong Hong, Zun Wang, Qi Wu, and Stephen Gould. Bridging the gap between learning in discrete and continuous environments for vision-and-language navigation. In *Proceedings of the IEEE/CVF conference on computer vision and pattern recognition*, pages 15439–15449, 2022. 2, 5

[16] Yanjia Huang, Mingyang Wu, Renjie Li, and Zhengzhong Tu. Vista: Generative visual imagination for vision-and-language navigation. *arXiv preprint arXiv:2505.07868*, 2025. 2

[17] Jacob Krantz and Stefan Lee. Sim-2-sim transfer for vision-and-language navigation in continuous environments. In *European conference on computer vision*, pages 588–603. Springer, 2022. 5

[18] Jacob Krantz, Erik Wijmans, Arjun Majumdar, Dhruv Batra, and Stefan Lee. Beyond the nav-graph: Vision-and-language navigation in continuous environments. In *European Conference on Computer Vision*, pages 104–120. Springer, 2020. 1, 2, 5

[19] Jacob Krantz, Aaron Gokaslan, Dhruv Batra, Stefan Lee, and Oleksandr Maksymets. Waypoint models for instruction-guided navigation in continuous environments. In *Proceedings of the IEEE/CVF International Conference on Computer Vision*, pages 15162–15171, 2021. 5

[20] Alexander Ku, Peter Anderson, Roma Patel, Eugene Ie, and Jason Baldridge. Room-across-room: Multilingual vision-and-language navigation with dense spatiotemporal grounding. *arXiv preprint arXiv:2010.07954*, 2020. 3, 5

[21] Jialu Li and Mohit Bansal. Improving vision-and-language navigation by generating future-view image semantics. In *Proceedings of the IEEE/CVF conference on computer vision and pattern recognition*, pages 10803–10812, 2023. 2

[22] Rui Liu, Xiaohan Wang, Wenguan Wang, and Yi Yang. Bird’s-eye-view scene graph for vision-language navigation. In *Proceedings of the IEEE/CVF International Conference on Computer Vision*, pages 10968–10980, 2023. 2

[23] Zhijian Liu, Ligeng Zhu, Baifeng Shi, Zhuoyang Zhang, Yuming Lou, Shang Yang, Haocheng Xi, Shiyi Cao, Yuxian Gu, Dacheng Li, et al. Nvila: Efficient frontier visual language models. In *Proceedings of the Computer Vision and Pattern Recognition Conference*, pages 4122–4134, 2025. 1

[24] Yuxing Long, Wenzhe Cai, Hongcheng Wang, Guanqi Zhan, and Hao Dong. Instructnav: Zero-shot system for generic instruction navigation in unexplored environment. *arXiv preprint arXiv:2406.04882*, 2024. 5

[25] Khanh Nguyen, Debadatta Dey, Chris Brockett, and Bill Dolan. Vision-based navigation with language-based assistance via imitation learning with indirect intervention. In *Proceedings of the IEEE/CVF Conference on Computer Vision and Pattern Recognition*, pages 12527–12537, 2019. 2

[26] Sonia Raychaudhuri, Saim Wani, Shivansh Patel, Unnat Jain, and Angel X Chang. Language-aligned waypoint (law) supervision for vision-and-language navigation in continuous environments. *arXiv preprint arXiv:2109.15207*, 2021. 5

[27] Stéphane Ross, Geoffrey Gordon, and Drew Bagnell. A reduction of imitation learning and structured prediction to no-regret online learning. In *Proceedings of the fourteenth international conference on artificial intelligence and statistics*, pages 627–635. JMLR Workshop and Conference Proceedings, 2011. 3

[28] Manolis Savva, Abhishek Kadian, Oleksandr Maksymets, Yili Zhao, Erik Wijmans, Bhavana Jain, Julian Straub, Jia Liu, Vladlen Koltun, Jitendra Malik, et al. Habitat: A platform for embodied ai research. In *Proceedings of the IEEE/CVF international conference on computer vision*, pages 9339–9347, 2019. 3

[29] Raphael Schumann, Wanrong Zhu, Weixi Feng, Tsu-Jui Fu, Stefan Riezler, and William Yang Wang. Velma: Verbalization embodiment of llm agents for vision and language navigation in street view. In *Proceedings of the AAAI Conference on Artificial Intelligence*, pages 18924–18933, 2024. 2

[30] Hanqing Wang, Wei Liang, Luc V Gool, and Wenguan Wang. Towards versatile embodied navigation. *Advances in neural information processing systems*, 35:36858–36874, 2022. 2

[31] Hanqing Wang, Wei Liang, Luc Van Gool, and Wenguan Wang. Dreamwalker: Mental planning for continuous vision-language navigation. In *Proceedings of the IEEE/CVF international conference on computer vision*, pages 10873–10883, 2023. 2

[32] Liuyi Wang, Xinyuan Xia, Hui Zhao, Hanqing Wang, Tai Wang, Yilun Chen, Chengju Liu, Qijun Chen, and Jiangmiao Pang. Rethinking the embodied gap in vision-and-language navigation: A holistic study of physical and visual disparities. In *Proceedings of the IEEE/CVF International Conference on Computer Vision*, pages 9455–9465, 2025. 1, 4

[33] Shuo Wang, Yongcai Wang, Wanting Li, Xudong Cai, Yucheng Wang, Maiyue Chen, Kaihui Wang, Zhizhong Su, Deying Li, and Zhaoxin Fan. Aux-think: Exploring reasoning strategies for data-efficient vision-language navigation. *arXiv preprint arXiv:2505.11886*, 2025. 5, 6

[34] Shuo Wang, Yongcai Wang, Wanting Li, Yucheng Wang, Maiyue Chen, Kaihui Wang, Zhizhong Su, Xudong Cai, Yeying Jin, Deying Li, et al. Monodream: Monocular vision-language navigation with panoramic dreaming. *arXiv preprint arXiv:2508.02549*, 2025. 1, 2, 5, 6, 8

[35] Zun Wang, Jialu Li, Yicong Hong, Yi Wang, Qi Wu, Mohit Bansal, Stephen Gould, Hao Tan, and Yu Qiao. Scaling data generation in vision-and-language navigation. In *Proceedings of the IEEE/CVF international conference on computer vision*, pages 12009–12020, 2023. 3, 5

[36] Zihan Wang, Xiangyang Li, Jiahao Yang, Yeqi Liu, and Shuqiang Jiang. Gridmm: Grid memory map for vision-and-language navigation. In *Proceedings of the IEEE/CVF International conference on computer vision*, pages 15625–15636, 2023. 2, 5

[37] Zihan Wang, Xiangyang Li, Jiahao Yang, Yeqi Liu, Junjie Hu, Ming Jiang, and Shuqiang Jiang. Lookahead exploration with neural radiance representation for continuous vision-language navigation. In *Proceedings of the IEEE/CVF conference on computer vision and pattern recognition*, pages 13753–13762, 2024. 2

[38] Zihan Wang, Xiangyang Li, Jiahao Yang, Yeqi Liu, and Shuqiang Jiang. Sim-to-real transfer via 3d feature fields for vision-and-language navigation. *arXiv preprint arXiv:2406.09798*, 2024. 5

[39] Meng Wei, Chenyang Wan, Xiqian Yu, Tai Wang, Yuqiang Yang, Xiaohan Mao, Chenming Zhu, Wenzhe Cai, Hanqing Wang, Yilun Chen, et al. Streamvln: Streaming vision-and-language navigation via slowfast context modeling. *arXiv preprint arXiv:2507.05240*, 2025. 1, 2, 3, 5, 6, 7

[40] Qiaoyun Wu, Xiaoxi Gong, Kai Xu, Dinesh Manocha, Jingxuan Dong, and Jun Wang. Towards target-driven visual navigation in indoor scenes via generative imitation learning. *IEEE Robotics and Automation Letters*, 6(1):175–182, 2020. 2

[41] Siying Wu, Xueyang Fu, Feng Wu, and Zheng-Jun Zha. Vision-and-language navigation via latent semantic alignment learning. *IEEE Transactions on Multimedia*, 26:8406–8418, 2024. 2

[42] Xuan Yao, Junyu Gao, and Changsheng Xu. Navmorph: A self-evolving world model for vision-and-language navigation in continuous environments. *arXiv preprint arXiv:2506.23468*, 2025. 5, 7

[43] Shuang Zeng, Dekang Qi, Xinyuan Chang, Feng Xiong, Shichao Xie, Xiaolong Wu, Shiyi Liang, Mu Xu, and Xing Wei. Janusvln: Decoupling semantics and spatiality with dual implicit memory for vision-language navigation. *arXiv preprint arXiv:2509.22548*, 2025. 3, 5, 6, 7

[44] Jiazhao Zhang, Kunyu Wang, Rongtao Xu, Gengze Zhou, Yicong Hong, Xiaomeng Fang, Qi Wu, Zhizheng Zhang, and He Wang. Navid: Video-based vlm plans the next step for vision-and-language navigation. *Robotics: Science and Systems*, 2024. 1, 2, 5

[45] Jiazhao Zhang, Anqi Li, Yunpeng Qi, Minghan Li, Jiahang Liu, Shaoan Wang, Haoran Liu, Gengze Zhou, Yuze Wu, Xingxing Li, et al. Embodied navigation foundation model. *arXiv preprint arXiv:2509.12129*, 2025. 5, 6

[46] Jiazhao Zhang, Kunyu Wang, Shaoan Wang, Minghan Li, Haoran Liu, Songlin Wei, Zhongyuan Wang, Zhizheng Zhang, and He Wang. Uni-navid: A video-based vision-language-action model for unifying embodied navigation tasks. *Robotics: Science and Systems*, 2025. 1, 2, 5, 6

[47] Pingrui Zhang, Yifei Su, Pengyuan Wu, Dong An, Li Zhang, Zhigang Wang, Dong Wang, Yan Ding, Bin Zhao, and Xuelong Li. Cross from left to right brain: Adaptive text dreamer for vision-and-language navigation. *arXiv preprint arXiv:2505.20897*, 2025. 2

[48] Yuanhan Zhang, Jinming Wu, Wei Li, Bo Li, Zejun Ma, Zizwei Liu, and Chunyuan Li. Video instruction tuning with synthetic data. *arXiv preprint arXiv:2410.02713*, 2024. 1

[49] Zekai Zhang, Weiye Zhu, Hewei Pan, Xiangchen Wang, Rongtao Xu, Xing Sun, and Feng Zheng. Activevln: Towards active exploration via multi-turn rl in vision-and-language navigation. *arXiv preprint arXiv:2509.12618*, 2025. 1